Resilience-based optimal post-disruption reconfiguration for traffic-power systems

Hongping Wang, Yi-Ping Fang, Enrico Zio

Resilience-based optimal post-disruption reconfiguration for traffic-power systems

Hongping Wang[a], Yi-Ping Fang[a,*], Enrico Zio[b,c]

[a] *Université Paris-Saclay, CentraleSupélec, Laboratoire Génie Industriel, 3 rue Joliot-Curie, Gif-sur-Yvette, France.*
[b] *Energy Department, Politecnico di Milano, 20156 Milano, Italy.*
[c] *Mines ParisTech, PSL Research University, CRC, Sophia Antipolis, France.*

Abstract

Due to the growing the penetration of electric vehicles (EV), road networks (RNs) and power networks (PNs) more rely on the normal functioning of each other. However, only a few of studies have discussed the potential negative consequences of adopting EVs during disaster. Moreover, the negative impact of EVs on the interdependent traffic-power systems has been rarely considered during restoration period. In this study, restoration plans for independent RNs and PNs, and interdependent traffic-power systems are investigated, respectively. For the restoring the traffic-power systems, a two-stage mixed integer optimization model is proposed to provide system optimal reconfiguration and operational solutions after disruptions. The objective of this model is to minimize the total system performance loss cost. The total system performance loss cost is quantified by cumulative unsatisfied gasoline vehicles (GVs) and EVs traffic demand for RNs, and shedded load cost for PNs. In tactical level, reconfiguration solutions (i.e., links reversing for RNs and line switching for PNs) are determined. In the operational level, the integrated system optimal dynamic traffic assignment and optimal power flow problem is solved to obtain the optimal traffic-power flow. In this model, RNs and PNs are coupled through EVs and the coordinately allocated spatiotemporal charging demand. A partial highway network in North Carolina (NC), USA and modified IEEE-14 bus system are used to illustrate the developed methods. The results show the added value of coordinately planing restoration for traffic-power systems. When EV penetration increases from

*Corresponding author, Email address: yiping.fang@centralesupelec.fr

0% to 100%, the total performance loss costs increase 46.7%. This result also hints that more FCSs should be deployed in this area.

Keywords: Reconfiguration, Restoration, Rraffic-power systems, Optimal traffic-power flow, Electric vehicles, Fast-charging stations, Spatiotemporal charging demand

---

Nomenclature

Indices

a	index of links
t	index of periods
s	index of destinations
e	index of energy levels for EVs
c	index of EV classes

The transportation network sets

$\mathcal{A}$	set of arcs
$\mathcal{N}$	set of nodes
$A(i)(B(i))$	set of links whose tail(head) node is i
$\mathcal{A}_R$	set of source arcs
$\mathcal{A}_S$	set of sink arcs
$\mathcal{A}_G$	set of general arcs
$\mathcal{A}_C$	set of charging arcs
$\mathcal{T}$	set of periods
$\mathcal{E}_c$	set of energy levels for the EVs belonging to class c
$\mathcal{C}$	set of electric vehicle classes

Parameters

ϕ	time value
p_a^{ev}	charging power of charging link a
$NC_a(t)$	number of chargers at charging link a during period t
δ	period length
L_a	physical length of link a
$k_{jam}/q_{max}/v_f$	jam density/ maximum flow/ free-flow speed
w	backward shock-wave speed, $w = q_{max} \cdot v_f/(q_{max} - k_{jam} \cdot v_f)$
α_a^t	average charging speed for charging link a during period t, $\alpha_a^t = p_a^{ev}/(\eta \cdot v_f)$
$If_a(t)$	inflow capacity of link a during period t
$Of_a(t)$	outflow capacity of link a during period t
$DG_a^s(t)$	cumulative gasoline vehicle travel demand between the entry of origin link a and destination s at the end of period t
$DE_{a,c}^{s,e}(t)$	cumulative c class EV travel demand of between the entry of origin link a and destination s with energy level e at the end of period t
ν_a	free-flow travel time on link a, $\nu_a = L_a/(\delta \cdot v_f)$
β_a	travel time required by the backward shock wave from the exit to the entry of link a, $\beta_a = L_a/(\delta \cdot w)$
N_h	number of links that can be reversed during restoration

Variables

$U_a(t)$	cumulative number of vehicles that enter link a by the end of period t
$V_a(t)$	cumulative number of vehicles that leave link a by the end of period t

$UG_a^s(t)$ cumulative number of GVs that enter link a to destination s by the end of period t

$VG_a^s(t)$ cumulative number of GVs that leave link a to destination s by the end of period t

$UE_{a,c}^{s,e}(t)$ cumulative number of EVs of class c with energy level e that enter link a to destination s by the end of period t under scenario o

$VE_{a,c}^{s,e}(t)$ cumulative number of EVs of class c with energy level e that leave link a to destination s by the end of period t

$x_{a,c}^{s,e}(t)$ occupancy of EVs of class c with energy level e at charging link a during period t

$\hat{x}_{a,c}^{s,e}(t)$ occupancy of EVs of class c with the **updated** energy level e at charging link a during period t

$h_{i,j}$ binary variable that is equal to 1 if the direction of road a is reversed, being 0 otherwise

The power network sets

$\mathcal{P}_N$ set of buses

$\mathcal{P}_L$ set of transmission lines

$\widetilde{\mathcal{P}}_L$ set of damaged transmission lines

$\Gamma(j)$ successor set of bus j

Parameters

p_j^{ramp} ramp limits of generators at bus j

c_j^b load shedding cost for the base load at bus j

c_j^{dc} load shedding cost for the EV charging load at bus j

$\underline{p}_j^g/\overline{p}_j^g$ lower/upper limit of power generation at bus j

$p_{j,t}^b$ base power demand at bus j during period t

N_u	number of lines that can be switched off during restoration

Variables

$p^g_{j,t}$	power generation at bus j during period t
$p^{dc}_{j,t}$	charging load at bus j during period t
$P_{i,j,t}$	power flow from buses i to j during period t
$u_{i,j}$	binary variable that is equal to 1 if line (i,j) is switched in, being 0 otherwise
$LS^{dc}_{j,t}$	binary variable that is equal to 1 if the load of the attached FCSs is shedded at bus j during period t, being 0 otherwise
$LS^{b}_{j,t}$	base load shedding at bus j during period t

EVs

Parameters

L^{max}_c	mileage of c class EV
E_c	the maximum energy level of c class EV
eta	average energy consumption efficiency for EVs

1. Introduction

High-impact and low-probability (HILP) incidents usually cause severe negative consequences on road networks (RNs) and power networks (PNs). 2003 North America blackout caused 50 million customers affected by this outages [1]. 65% of New Jersey's customers were experienced the disconnections from the power systems during Hurricane Sandy in 2012 [2]. In July 2021, heavy rainfall and floods hit Henan, China [3]. This HILP event devastated the local critical infrastructures, including the transportation and the power systems. The estimated direct economic loss is on the order of RMB 88.5 billion. This has highlighted an urgent need for strengthen the resilience of the RNs and PNs against such HILP incidents. The concept of resilience is defined in various explanations [4, 5, 6], however, many of them share the general idea that resilience is the ability of a system to prepare

for, absorb, recover from, and adapt to disturbances[7]. Restoration as one of the most effective manners to enhance the system resilience after disruptions has received increasing attention. A large body of work have been done to investigate the optimal restoration after disruptions for RNs and PNs, sparately.

For PNs, reconfiguration as an effective strategy to restore the service and to enhance the system resilience against emergencies has been intensively investigated in the literature [8, 9, 10]. Generally, maximizing the network resilience/minimizing system performance loss and minimizing the number of line switches/minimizing restoration cost are included in the objectives of these models. For example, Sekhavatmanesh and Cherkaoui [11] developed the concept of multiagent automation in smart grids, which was applied to restore a maximum of loads with minimum switching operations service after disruptions; Sabouhi et. al [12] presented an operational network reconfiguration strategy during a high wind event to maximize network resilience and minimize the number of line switches. Sometimes, islanding or not after disruptive events are also treated differently. Agrawal et. al [13] developed a self-healing algorithm to restore maximum priority loads by reconfiguring network without intentional islanding during blackouts. Guimaraes et. al [14] proposed a three-stage algorithm for the dynamic reconfiguration of distribution networks with islanding. The three stages include calculating the network reconfiguration solutions in each hour, reducing the number of configurations and generating the optimal sequence of topologies. Li et. al [15] presented a concept of fully decentralized multi-agent system to build a restoration service framework for distribution network. Based on this concept, a network reconfiguration algorithm is proposed for restore service, where reconfiguration with intentional islanding was considered. Except reconfiguration, other corrective actions, such as generator re-dispatch, control of distributed energy storage systems (ESSs), and on-load tap changers, also can be considered as supplementary strategies to enhance the resilience of the power systems. Liberati et. al [16] proposed control system optimizes grid operations through network reconfiguration, control of distributed energy storage systems, and on-load tap changers. Sekhavatmanesh and Cherkaoui [17] developed an analytical and global optimization model to find the most efficient restoration plan minimizing the number of de-energized nodes with the minimum number of corrective actions. The considered corrective actions included network reconfiguration, the tap setting modification of voltage regulation devices, the nodal load-rejection, and the active/reactive power dis-

patch of distribution generators. Zhang et. al [18] introduced two-stage stochastic models to deal with the uncertainty in generation and demand during the recovery process. Switching transmission lines and generator re-dispatch strategies were used to maximize load shed recovery in the bulk transmission network. Nazemi and Dehghanian [19] introduced a framework for modeling and characterization of seismic hazards, vulnerability assessment of electric systems to the earthquake. The generation re-dispatch strategy and corrective network topology control were considered to maximize the load outage recovery after disasters.

For the RNs, short-term and long-term recovery periods usually are investigated separately. For short-term recovery period, reconfiguring network topology and controlling traffic lights are frequently discussed manner to increase the resilience of RNs after disruptive events. Wang and Wang [20] developed an integrated reconfiguration strategy that reconfigures both the supply and demand sides of transportation systems. The traffic demand was reconfigured using a heterogeneous fleet of vehicles and the network topology was reconfigured through a heterogeneous contraflow control. Later on, they further presented a framework [21] for resilience analysis including measurement and improvement. Two strategies were used to maximize the system resilience. They were integrated reconfiguration of both traffic supply and demand by reducing traffic demand through combining different traffic modes and a contraflow control. Chiou [22] proposed a period-dependent traffic responsive signal control model to enhance resilience of urban RNs. Koutsoukos et. al [23] developed a modeling and simulation integration platform for experimentation and evaluation of resilient transportation systems. Resilient traffic signal control in the presence of denial-of-service attacks was studied in the case studies. For long-term recovery period, scheduling repair crew, allocating resources and determining restoration priority of components in the RNs are generally the main focuses. Wu et. al [24] proposed a methodology to assess the resilience of transportation networks and a restoration priority measure to support post-earthquake restoration of damaged bridges. Zhao and Zhang [25] proposed a bi-objective bi-level optimization framework to determine an optimal transportation network restoration plan. The lower-level problem uses elastic user equilibrium to model the imbalance between demand and supply. The upper-level problem, formulated as bi-objective mathematical programming, determines optimal resource allocation for roadway restoration.

In recent years, treating the independent RNs and PNs as a whole and

the problems how to model and operate them together have gained much of attention [26, 27]. However, only a few studies have investigated the problem of how to restore them after disruptions to minimize the whole system performance loss subjecting to physical constraints from both networks. Moreover, most of these studies only focused on minimizing the performance loss of PNs and only considered the constraints of RNs. Their topics generally are about how to route and schedule of mobile energy storage systems (MESSs)/mobile energy sources [28, 29, 30, 31], sometimes coordinating with repair crews [29, 30, 31] and line switch strategies [29, 30]. One of the key issues of restoring traffic-power networks is to figure out and properly model the objects that connect and make influence on the both networks. Wang et. al [32] considered the PNs and urban RNs coupled through traffic lights and mobile emergency resources (i.e., mobile sources and repair crews). The availability of mobile emergency resources relates to their dispatch in the RNs, while the effect of traffic lights is also considered. They developed a service restoration method to maximize the efficiency of both PNs restoration and RNs. Yao et. al [33] proposed a rolling integrated service restoration strategy to minimize the total system cost by coordinating the scheduling of MESS fleets, resource dispatching of microgrids, and network reconfiguration of PNs. The integrated strategy takes into account damage and repair to both the roads in RNs and the branches in PNs. Li et. al [34] presented an optimization model for joint post-disaster DS restoration, considering coordinated dispatching with electric buses. By assuming that the PN can rent some electric buses. Idle buses are placed at designated areas and feed power back to the grid via charging equipment in case of need. The schedule of the remaining buses should meet the passenger transport demand. The objective was to maximize the total benefits and minimize the bus rental cost.

Different from the existing work, this paper consider that the RNs and PNs are coupled through electric vehicles (EVs) and their charging demand. This is because EVs and fast-charging stations (FCSs) are being increasingly deployed around the world [35]. It makes PNs and RNs inevitably accelerate the coupling together. On the other hand, EVs probably threatened by outages in FCSs because of the natural disaster have raised a few of researchers' concerns [36, 37]. However, this problem and its solution approaches have not been solidly investigated yet, especially in the context of enhancing the resilience of the interdependent traffic-power networks. In this paper, we focus on the problem of how to jointly reconfigure and operate the traffic-power networks so that the total system performance loss can be minimized

for short-term recovery period. Specifically, road links in RNs and lines in PNs may be damaged simultaneously after a natural disaster or a malicious attack. In RNs, vehicles in RNs may need to bypass and the RNs' performance therefore decrease. Due to the extra distance, both the number of EVs and the amount of charging demand for each EV may increase in FCSs. Such charging demand can become a burden for PNs during the restoration after the disruptive event. On the other hand, the PNs may need to shed the EV charging load due to the reduced flow and generation capacity after the disruptions. Consequently, the unavailability of the service in FCSs can further influence the charging demand patterns and decrease the performance of the RNs. To fill the above mentioned research gaps, in this paper, we develop a two-stage mixed integer optimization model to minimize the system performance loss after disruptions. In the first stage, reconfiguration solutions over the whole studied horizon for the traffic-power systems are provided to enhance the system resilience after a disruptive event. In the second stage, an integrated traffic-power systems model is developed to model the dynamic interaction between RNs and PNs through EVs and spatial and temporal charging demand. The results show the added value of coordinately reconfiguring traffic-power systems and managing EV charging demand.

The main contributions of this paper are summarized as follows:

1. To best our knowledge, it is the first work that consider the negative impact of EVs and interdependent traffic-power systems in terms of restoration and network topology control.

2. The strategies of link directions reversing in the RN and line switching in the PN are mathematically formulated in an independent traffic-power system model, and in independent RN and PN models, respectively.

3. For the interdependent traffic-power systems, a two-stage mixed integer optimization model is presented to minimize the system performance loss after disruptions. The tactical level problem is formulated as an integrated system optimal dynamic traffic assignment and DC power flow problem considering EVs. The optimal topology of traffic-power systems are served as the operational level problem.

4. Different response source levels, EV penetration levels and decision-making environments are compared in the case study.

The remainder of the article is structured as follows. Section 2 formulated the reconfiguration problems in independent RN and PN models, as well as in the interdependent traffic-power system model. Section 3 illustrates a

case study to show the application of the proposed models and compares the solutions under different response resource levels, EV penetration levels and decision-making environments. Finally, Section 4 provides some concluding remarks and future research directions.

2. Reconfiguring infrastructures

In this section, reconfiguration problem in independent RNs, independent PNs and interdependent traffic-power systems are formulated.

2.1. Reconfiguring electrified highway networks

In this subsection, we first present an electrified traffic system model considering the critical characteristics of EVs and FCSs, which is based on link transmission model. Then, reconfiguration problem after disruption is formulated based on this electrified traffic model.

2.1.1. Electrified traffic model with EVs and FCSs

In this model we assume that the electricity consumed by an EV is linearly related to the distance traveled. The electricity amount charged by an EV is linearly related to the charging time. All EV batteries have the same energy consumption efficiency, similar to Ref. [**?**].

A RN with multiple sources (origins) and sinks (destinations) is denoted as $G(\mathcal{N}, \mathcal{A})$, where $\mathcal{N}$ and $\mathcal{A}$ are the sets of nodes and links, respectively. Links in the RN are classified into four types: source $\mathcal{A}_R$, sink $\mathcal{A}_S$, general $\mathcal{A}_G$ and charging $\mathcal{A}_C$ links. Nodes are classified into two types: source-sink $\mathcal{N}_{SR}$ and general $\mathcal{N}_G$ nodes. Within the RN, each source-sink node attaches only one source and one sink link. All charging, source and sink links are dummy with lengths 0. All source and sink links are with infinite outflow, inflow and storage capacities. For SO-DTA problems, the outflow capacity of all sink links are assumed to be 0, which means that all vehicles are collected upon their arrival. The time horizon H is discretized into a finite set of periods $\mathcal{T} = \{t = 1, 2, \cdots, T\}$. T is calculated according to $T = H/\delta$, where δ is the period length. The period length should be equal to or smaller than the smallest link travel time so that vehicles take at least one time unit to traverse a link [38].

A triangular fundamental diagram is used in LTM, which is an approximation and describes a macroscopic property of roads [38]. The diagram is defined by three parameters: a jam density (k_{jam}), a maximum flow (q_{max})

and a fixed-free flow speed (v_f). The backward shock-wave speed w can be obtained by $w = q_{max} \cdot v_f/(q_{max} - k_{jam} \cdot v_f)$.

Given a certain class of EV denoted as c, its battery capacity is B_c kWh and the energy consumption efficiency is η kWh/mile, then, the mileage of this class EV is $L_c^{max} = B_c/\eta$ miles. We discretize its mileage into integer energy levels (ELs). When this EV has full battery, it has the maximum EL $E_c = L_c^{max}/(\delta \cdot v_f)$. Once this EV traveled $\delta \cdot v_f$ miles, its ELs decrease one EL, i.e., 1 EL $= \delta \cdot v_f$ miles. Assuming there are C EV classes represented as $\mathcal{C} = \{\mathcal{E}_1, \mathcal{E}_2, \cdots, \mathcal{E}_C\}$. Each element $\mathcal{E}_c$ in set $\mathcal{C}$ is a set, which contains the energy levels that EV of class c could have, denoted as $\mathcal{E}_c = \{1, 2, \cdots, E_c\}$.

The LTM updates the traffic flow evolution by calculating the cumulative number of vehicles at entry and exit of each link in each period.

The Newell's simplified theory is used in LTM to calculate sending $S_a(t)$ and receiving $R_a(t)$ capacities of link a:

$$S_a(t) = \min\{U_a(t - \nu_a) - V_a(t-1), Of_a(t)\} \tag{1a}$$

$$R_a(t) = \min\{V_a(t - \beta_a) + L_a \cdot k_{jam} - U_a(t-1), If_a(t)\} \tag{1b}$$

where $U_a(t)/V_a(t)$ denotes the cumulative number of vehicles that enter/leave link a by the end of period t. $If_a(t)$ and $Of_a(t)$ are the inflow capacity at the entering point and outflow capacity at the leaving point of link a during period t. They can be obtained by $\delta \cdot q_{max}$ at the corresponding location and period. L_a is the length of link a. ν_a is the free-flow travel time on link a and β_a is the travel time required by the backward shock wave from the exit to the entry of link a. They can be obtained by $\nu_a = L_a/(\delta \cdot v_f)$ and $\beta_a = L_a/(\delta \cdot w)$, respectively.

The inflow and outflow of link a during interval t are constrained by its corresponding sending and receiving capacities:

$$U_a(t) - U_a(t-1) \leq R_a(t), \forall a \in \mathcal{A}\backslash\{\mathcal{A}_C\}, \forall t \tag{2a}$$

$$V_a(t) - V_a(t-1) \leq S_a(t), \forall a \in \mathcal{A}\backslash\{\mathcal{A}_C\}, \forall t \tag{2b}$$

Substituting Eqs. (1) and (1b) into the system of inequality (2), we obtain the following system of linear LTM-based flow constraints:

$$V_a(t) \leq U_a(t - \nu_a), \forall a \in \mathcal{A}\backslash\{\mathcal{A}_C\}, \forall t \tag{3}$$

$$V_a(t) - V_a(t-1) \leq Of_a(t), \forall a \in \mathcal{A}\backslash\{\mathcal{A}_C\}, \forall t \tag{4}$$

$$U_a(t) - U_a(t-1) \leq If_a(t), \forall a \in \mathcal{A}\backslash\{\mathcal{A}_C\}, \forall t \tag{5}$$

$$U_a(t) - V_a(t-\beta_a) \leq L_a k_{jam}, \forall a \in \mathcal{A}\backslash\{\mathcal{A}_C\}, \forall t \tag{6}$$

In eLTM-based model, both EVs and conventional vehicles are considered as follows :

$$U_a(t) = \sum_{s\in\mathcal{N}_S} UG_a^s(t) + \sum_{s\in\mathcal{N}_S}\sum_{c\in\mathcal{C}}\sum_{e\in\mathcal{E}_c} UE_{a,c}^{s,e}, \forall a \in \mathcal{A}\backslash\{\mathcal{A}_C\}, \forall t \tag{7a}$$

$$V_a(t) = \sum_{s\in\mathcal{N}_S} VG_a^s(t) + \sum_{s\in\mathcal{N}_S}\sum_{c\in\mathcal{C}}\sum_{e\in\mathcal{E}_c} VE_{a,c}^{s,e}, \forall a \in \mathcal{A}\backslash\{\mathcal{A}_C\}, \forall t \tag{7b}$$

where $UE_{a,c}^{s,e}(t)/VE_{a,c}^{s,e}(t)$ denotes the cumulative number of EVs that belong to type c with EL e that enter/leave link a to destination s by the end of interval t under scenario o; $UG_a^s(t)/VG_a^s(t)$ denotes the cumulative number of GVs that enter/leave link a to destination s by the end of interval t under scenario o.

Substituting Eq. (7) into the inequalities in Eqs. (3) - (6), we can have the following constraints for the mixed traffic of EVs and GVs:

$$\sum_{s\in\mathcal{N}_S}[VG_a^s(t) - VG_a^s(t-1)] + \sum_{s\in\mathcal{N}_S}\sum_{c\in\mathcal{C}}\sum_{e\in\mathcal{E}_c}[VE_{a,c}^{s,e}(t) - VE_{a,c}^{s,e}(t-1)] \leq Of_a(t), \forall a \in \mathcal{A}\backslash\{\mathcal{A}_C\}, \forall t, s \tag{8}$$

$$\sum_{s\in\mathcal{N}_S}[UG_a^s(t) - UG_a^s(t-1)] + \sum_{s\in\mathcal{N}_S}\sum_{c\in\mathcal{C}}\sum_{e\in\mathcal{E}_c}[UE_a^s(t) - UE_a^s(t-1)] \leq If_a(t), \forall a \in \mathcal{A}\backslash\{\mathcal{A}_C\}, \forall t, s \tag{9}$$

$$\sum_{s\in\mathcal{N}_S}\sum_{c\in\mathcal{C}}\sum_{e\in\mathcal{E}_c}[UE_{a,c}^{s,e}(t) - VE_{a,c}^{s,e}(t-\beta_a)] + \sum_{s\in\mathcal{N}_S}[UG_a^s(t) - VG_a^s(t-\beta_a)] \leq L_a k_{jam}, \forall a \in \mathcal{A}\backslash\{\mathcal{A}_C\}, \forall t, s \tag{10}$$

For GVs, the cumulative outflow disaggregated by destinations and scenarios should also be constrained by the boundary condition at the inflow. Hence, we have

$$\sum_{s\in\mathcal{N}_S} VG_a^s(t) \leq \sum_{s\in\mathcal{N}_S} UG_a^s(t-\nu_a), \forall a \in \mathcal{A}\backslash\{\mathcal{A}_C\}, \forall t \tag{11}$$

For EVs, the disaggregated cumulative outflow should also be constrained

by the battery condition at the inflow. Hence, we have

$$VE_{a,c}^{s,e}(t) \leq UE_{a,c}^{s,e+\rho_a}(t-\nu_a), \forall a \in \mathcal{A}\backslash\{\mathcal{A}_C\}, e \in \mathcal{E}_c \cap \{e \leq E_c - \rho_a\}, \forall s, c, t \tag{12a}$$

$$VE_{a,c}^{s,e}(t) = 0, \forall a \in \mathcal{A}\backslash\{\mathcal{A}_C\}, e \in \mathcal{E}_c \cap \{e > E_c - \rho_a\}, \forall s, c, t \tag{12b}$$

where, ρ_a is the ELs required to traverse link a and it is calculated by $\rho_a = L_a/(\delta \cdot v_f)$. Eq. (12a) guarantees that outflow should be less than or equal to the inflow. It also guarantees that the outflow ELs are updated from inflow after EVs traversed the corresponding links. Eq. (12b) ensures that all EV ELs should be less than their maximum ELs.

The traffic demand is satisfied by letting the cumulative inflows of source links equal the cumulative demands:

$$UG_a^s(t) = DG_a^s(t), \forall a \in \mathcal{A}_R, \forall s, t \tag{13a}$$

$$UE_{a,c}^{s,e}(t) = DE_{a,c}^{s,e}(t), \forall a \in \mathcal{A}_R, e \in \mathcal{E}_c, \forall s, c, t \tag{13b}$$

where $DG_a^s(t)/DE_{a,c}^{s,e}(t)$ represents the cumulative GVs/EVs travel demand between the entry of origin link a and destination s at the end of period t.

The inflow and outflow of a general node should be restricted by the following flow conservation constraints:

$$\sum_{a \in B(i)} VG_a^s(t) = \sum_{b \in A_(i)} UG_a^s(t), \forall i \in \mathcal{N}/\{\mathcal{N}_{SR}\}, \forall s, t \tag{14a}$$

$$\sum_{a \in B(i)} VE_{a,c}^{s,e}(t) = \sum_{b \in A_{(i)}} UE_{a,c}^{s,e}(t), \forall i \in \mathcal{N}/\{\mathcal{N}_{SR}\}, \forall e \in \mathcal{E}_c, \forall s, c, t \tag{14b}$$

where $A(i)/B(i)$ represents the set of links whose tail/head node is i.

For EVs, the current occupancy on charging link a should be limited by the maximum number of chargers on this link:

$$\sum_{s \in \mathcal{N}_S} \sum_{c \in \mathcal{C}} \sum_{e \in \mathcal{E}_c} [UE_{a,c}^{s,e}(t) - VE_{a,c}^{s,e}(t)] \leq NC_a(t), \forall a \in \mathcal{A}_C, \forall t \tag{15}$$

where $NC_a(t)$ is the physical number of type a chargers on charging link a during period t.

The following equations are used to update the current occupancy and

their ELs on a charging link:

$$\begin{aligned}\hat{x}_{a,s}^{s,e}(t) = x_{a,s}^{s,e}(t-1) + [UE_{a,c}^{s,e}(t-1) - UE_{a,c}^{s,e}(t-2)] - \\ [VE_{a,c}^{s,e}(t-1) - VE_{a,c}^{s,e}(t-2)], \forall a \in \mathcal{A}_C, \forall e \in \mathcal{E}_c, \forall s, c, t\end{aligned} \tag{16}$$

where $\hat{x}_{a,s}^{s,e}(t)$ and $x_{a,s}^{s,e}(t)$ are the number of EVs before and after their ELs have been updated on charging link a.

Based on the obtained occupancies, the following equations are used to model their charging process where ELs of EVs linearly increase with time on charging links:

$$x_{a,c}^{s,E_c}(t) = \sum_{l=0}^{\alpha_a^t} \hat{x}_{a,c}^{s,E_c-l}(t), \forall a \in \mathcal{A}_C, \forall s, c, t \tag{17a}$$

$$x_{a,c}^{s,e}(t) = \hat{x}_{a,c}^{s,e-\alpha_a^t}(t), \quad \forall a \in \mathcal{A}_C, \forall e \in \{\alpha_a^t \le e < E_c\}, \forall s, c, t \tag{17b}$$

$$x_{a,c}^{s,e}(t) = 0, \forall a \in \mathcal{A}_C, \forall e \in \{e < \alpha_a^t\}, \forall s, c, t \tag{17c}$$

where α_a^t represents the average charging speed for charging link a during period t, which translates to how many energy levels can be supplied using type a charger during a period δ. Assuming the charging power of charging link a is p_a^{ev}, then, α_a^t can be calculated by $\frac{p_a^{ev} \cdot \delta}{\eta \cdot \delta \cdot v_f} = \frac{p_a^{ev}}{\eta \cdot v_f}$. Eqs. (17a) and (17c) constrain the upper and lower boundaries of the updated ELs. Eq. (17b) describe the process of linear increase in ELs.

Additionally, the outflow disaggregated by each EL on charging link a should be less than its occupancy, as formulated in Eq. (18):

$$VE_{a,c}^{s,e}(t) - VE_{a,c}^{s,e}(t-1) \le x_{a,c}^{s,e}(t), \forall a \in \mathcal{A}_C, \forall e \in \mathcal{E}_c, \forall s, c, t \tag{18}$$

The occupancies on charging links are nonnegative, which is formulated as follows:

$$x_{a,c}^{s,e}(t) \ge 0, \ \hat{x}_{a,c}^{s,e}(t) \ge 0, \forall a \in \mathcal{A}_C, \forall e \in \mathcal{E}_c, \forall s, c, t, \tag{19}$$

The cumulative flows should be nonnegative and nondecreasing:

$$VG_a^s(t) - VG_a^s(t-1) \ge 0, \forall a \in \mathcal{A}, \forall s, t \tag{20a}$$

$$VE^{s,e}_{a,c}(t) - VE^{s,e}_{a,c}(t-1) \geq 0, \forall a \in \mathcal{A}, \forall e \in \mathcal{E}_c, \forall s, c, t \tag{20b}$$

$$UG^{s}_{a}(t) - UG^{s}_{a}(t-1) \geq 0, \forall a \in \mathcal{A}, \forall s, t \tag{21a}$$

$$UE^{s,e}_{a,c}(t) - UE^{s,e}_{a,c}(t-1) \geq 0, \forall a \in \mathcal{A}, \forall e \in \mathcal{E}_c, \forall s, c, t \tag{21b}$$

The following constraints force the initial cumulative flows to be 0:

$$UG^{s}_{a}(0) = VG^{s}_{a}(0) = 0, \forall a \in \mathcal{A}, \forall s \tag{22a}$$

$$UE^{s,e}_{a,c}(0) = VE^{s,e}_{a,c}(0) = 0, \forall a \in \mathcal{A}, \forall e \in \mathcal{E}_c, \forall s, c \tag{22b}$$

2.1.2. Modeling reconfiguration strategy in traffic-power system model

To mitigate the impacts after disruptions, we consider the strategy of contraflow to reconfigure the topology of the highway networks. Contraflow can be easily implemented by reversing the direction of lanes of highway networks. Fig. 2.1.2 shows how the contraflow assists increasing the throughput of the network after disruptions. Assuming that there are 20 vehicles per minute starting from nodes O to D and 10 vehicles per minute from nodes D to O. Node M serves as transshipment. The number along each link represents the time required to traverse the link at a free-flow speed. Fig. 1(a) shows that there are 20 and 40 vehicles arriving at nodes O and D, respectively, after 6 minutes, when each link works normally. If the link from nodes O to D fails, the arrivals on node D decrease to 20 vehicles, as shown in Fig. 1(b). However, if we reverse the direction of the link from nodes D to O, the total number of arrivals can be increased from 40 to 50 vehicles after the disruption, as shown in Fig. 1(c). This example shows that reconfiguring the highway network after disruption could effectively reduce the system performance loss. Another example in Ref. [39] can be found illustrating how contraflow strategy increases the network outbound capacity and mitigates the congestion.

To model the contraflow strategy, we define that each link in the highway network has and only has one unique opposite link corresponding to it. For example, there are two links a_1 and a_2 from nodes O to D in Fig. 2.1.2. Their corresponding opposite links are $\hat{a}_1$ and $\hat{a}_2$, respectively. Meanwhile, links a_1 and a_2 are the opposite links of links $\hat{a}_1$ and $\hat{a}_2$. Mathematically, we use variable h_a to denote whether link a is changed to the opposite direction or not. $\hat{a}$ represents the unique opposite link of link a. If the direction of the link is reversed, the outflow capacity, the inflow capacity and the maximum

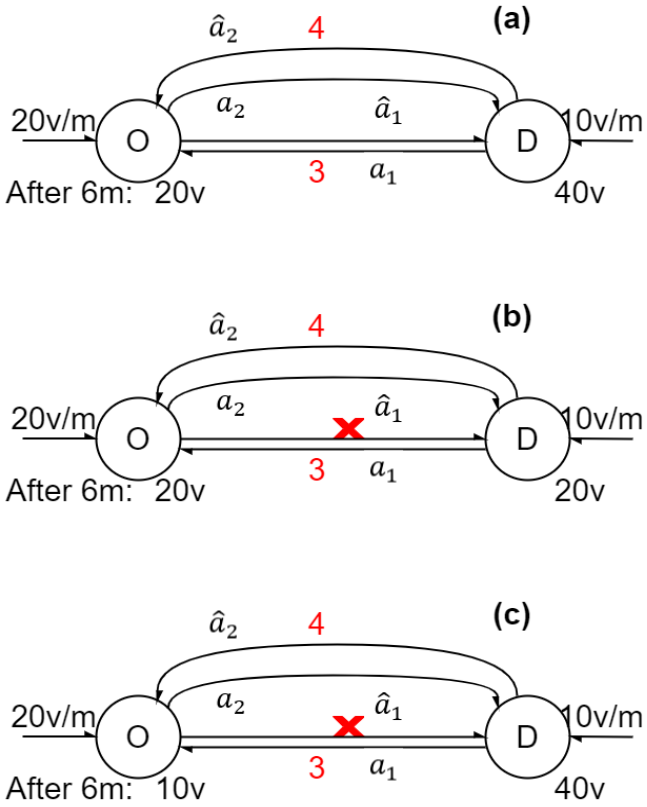

Figure 1: Contraflow illustration: (a) Normal condition (b) After disrutption (c) After reconfiguration

number of vehicles that can be present on that link of direction will be correspondingly reconfigured. Therefore, Eqs. (8) - (10) are reformulated as follows:

$$\sum_{s\in\mathcal{N}_S}[VG_a^s(t)-VG_a^s(t-1)]+\sum_{s\in\mathcal{N}_S}\sum_{c\in\mathcal{C}}\sum_{e\in\mathcal{E}_c}[VE_{a,c}^{s,e}(t)-VE_{a,c}^{s,e}(t-1)] \leq (1-h_a)\cdot Of_a(t)+h_{\hat{a}}\cdot Of_{\hat{a}}(t), \forall a\in\mathcal{A}\backslash\{\mathcal{A}_C\}, \forall t, s \tag{23}$$

$$\sum_{s\in\mathcal{N}_S}[UG_a^s(t)-UG_a^s(t-1)]+\sum_{s\in\mathcal{N}_S}\sum_{c\in\mathcal{C}}\sum_{e\in\mathcal{E}_c}[UE_a^s(t)-UE_a^s(t-1)] \leq (1-h_a)\cdot If_a(t)+h_{\hat{a}}\cdot If_{\hat{a}}(t), \forall a\in\mathcal{A}\backslash\{\mathcal{A}_C\}, \forall t,s \tag{24}$$

$$\sum_{s\in\mathcal{N}_S}\sum_{c\in\mathcal{C}}\sum_{e\in\mathcal{E}_c}[UE_{a,c}^{s,e}(t)-VE_{a,c}^{s,e}(t-\beta_a)]+\sum_{s\in\mathcal{N}_S}[UG_a^s(t)-VG_a^s(t-\beta_a)] \leq (1-h_a)L_ak_{jam}+h_{\hat{a}}L_{\hat{a}}k_{jam}, \forall a\in\mathcal{A}\backslash\{\mathcal{A}_C\}, \forall t,s \tag{25}$$

Eq. (23) states that the outflow on link a are constrained by the status of links a and $\hat{a}$. If $h_a=0$ and $h_{\hat{a}}=0$, no link is reversed and the outflow capacity on the direction of original link a is unchanged, i.e., outflow capacity of link a; If $h_a=1$ and $h_{\hat{a}}=1$, both links are reserved and the outflow capacity is modified to the outflow capacity of link $\hat{a}$; If $h_a=1$ and $h_{\hat{a}}=0$, the direction of link a is reversed and the outflow capacity becomes 0; If $h_a=0$ and $h_{\hat{a}}=1$, the direction of the opposite link $\hat{a}$ is reversed and the outflow capacity increase to the sum of outflow capacities of links a and $\hat{a}$. Similarly, we can have Eqs. (24) and (25) to constrain the inflow and maximum occupancies on the direction of original link a after reconfiguration.

$$h_a, h_{\hat{a}}=\{0,\ 1\}, \forall a,\hat{a}\in\mathcal{A}\backslash\{\mathcal{A}_C\} \tag{26}$$

$$\sum_a h_a\leq N_h, \forall a\in\mathcal{A}\backslash\{\mathcal{A}_C\} \tag{27}$$

Eq. (26) guarantees that h_a and $h_{\hat{a}}$ are binary variables. Eq. (27) constrains the total number of links that can be reversed. This constraint reflects the limited resources that can be used to emergency response to the disruption, in practice.

The emergency response problem is formulated as follows:

$$\min_{\boldsymbol{x}\in\Psi} P_T=\sum_{s\in\mathcal{N}_S}\sum_{t\in\mathcal{T}}\sum_{a\in\mathcal{A}_S}[DG_a^s(t)-UG_a^s(t)+\sum_{c\in\mathcal{C}}\sum_{e\in\mathcal{E}_c}(DE_{a,c}^{s,e}(t)-UE_{a,c}^{s,e}(t))]\cdot\phi \tag{28}$$

where $\Omega=\{\boldsymbol{x}|$ Subject to constraints (11)-(27)$\}$. ϕ denotes the time value. The objective of the transportation operator is to minimize the system performance loss cost after disruptions within a certain period. The system performance loss is measured by the unsatisfied traffic demand. In this paper, it is calculated by the cumulative difference between the target demand (i.e., $DG_a^s(t)$ and $DE_{a,c}^{s,e}(t)$) and the number of vehicles arrived at their des-

tinations (i.e., $UG_a^s(t)$ and $UE_{a,c}^{s,e}(t)$, $a \in \mathcal{N}_S$). In Eq. (28)The first term is the cumulative unsatisfied GVs travel demand and the second term is the cumulative unsatisfied EVs travel demand.

2.2. Reconfiguring power system

We consider a PN $\mathcal{G}_P(\mathcal{P}_N, \mathcal{P}_L)$, where $\mathcal{P}_N$ and $\mathcal{P}_L$ represent the sets of buses and branches, respectively. $\widetilde{\mathcal{P}}_L$ represents the set of damaged transmission lines after a disruption, $\widetilde{\mathcal{P}}_L \subset \mathcal{P}_L$. $\Gamma^-(j)$ and $\Gamma^+(j)$ denote the sets of predecessors and successors of bus j, respectively.

After the disruption, the objective of independent system operator is to minimize the cost of shedding unsatisfied load, which is formulated as follows:

$$\min P_P = \sum_j \sum_t c_j^b \cdot LS_{j,t}^b + c_j^{dc} \cdot LS_{j,t}^{dc} \cdot p_j^{dc}(t) \tag{29}$$

where c_j^b and c_j^{dc} are cost of shedding base load and EV charging load, respectively; $LS_{j,t}^b$ is a continuous variable representing the amount of unsatisfied base demand at bus j in period t; $LS_{j,t}^{dc}$ is a binary variable denoting where the charging demand $p_j^{dc}(t)$ at bus j in period t is shedded or not.

The power flow in the transmission systems are subjected to the following constraints:

$$p_{j,t}^g + \sum_{i \in \Gamma^-(j)} P_{i,j,t} - \sum_{k \in \Gamma^+(j)} P_{j,k,t} = p_{j,t}^b - LS_{j,t}^b + (1 - LS_{j,t}^{dc}) \cdot p_j^{dc}(t), \forall j \in \mathcal{P}_N \tag{30}$$

$$-\bar{P}_{i,j} \cdot u_{i,j} \leq P_{i,j,t} \leq \bar{P}_{i,j} \cdot u_{i,j}, \forall (i,j) \in \mathcal{P}_l \backslash \{\widetilde{\mathcal{P}}_L\}, \forall t \tag{31}$$

$$P_{i,j,t} = 0, \forall (i,j) \in \{\widetilde{\mathcal{P}}_L\}, \forall t \tag{32}$$

$$B_{i,j} \cdot (\theta_{i,t} - \theta_{j,t}) - P_{i,j,t} + (1 - u_{i,j}) \cdot M_{i,j} \geq 0, \forall (i,j) \in \mathcal{P}_L \backslash \{\widetilde{\mathcal{P}}_L\}, \forall t \tag{33}$$

$$B_{i,j} \cdot (\theta_{i,t} - \theta_{j,t}) - P_{i,j,t} - (1 - u_{i,j}) \cdot M_{i,j} \leq 0, \forall (i,j) \in \mathcal{P}_L \backslash \{\widetilde{\mathcal{P}}_L\}, \forall t \tag{34}$$

$$-p_j^{ramp} \leq p_{j,t}^g - p_{j,t-1}^g \leq p_j^{ramp}, \forall j \in \mathcal{P}_N, \forall t \in \mathcal{T} \tag{35}$$

$$0 \leq LS_{j,t}^b \leq p_{j,t}^b, \forall j \in \mathcal{P}_N \tag{36}$$

$$0 \leq P_{j,t}^g \leq \bar{p}_j^g, \forall j \in \mathcal{P}_j \tag{37}$$

$$\sum_{(i,j) \in \mathcal{P}_L} (1 - u_{i,j}) \leq N_u \tag{38}$$

$$u_{i,j} = 0,\ 1, \forall (i,j) \in \mathcal{P}_L \tag{39}$$

$$LS^{dc}_{j,t} = \{0,1\}, \forall j \in \mathcal{P}_N \tag{40}$$

Constraint (30) relaxes the power flow balance constraint at each bus by allowing to shed unsatisfied demand. Constraint (31) guarantees that the power flow on transmission lines do not exceed their capacities if they function. Constraint (32) enforces the amount of power flow on the damaged lines to be 0. Constraints (33)-(34) denote Kirchhoff's power flow equations, where power flow are limited by lines' susceptance and the phase angle difference between the two end buses. It is necessary to include the big-M in the equations. If the constraint is directly written as $B_{i,j} \cdot (\theta_{i,t} - \theta_{j,t}) = P_{i,j,t} \cdot (1 - u_{i,j})$: when the line's status is not switched and in service (i.e., $u_{i,j} = 1$), this equation works normally; when the line is switched off (i.e., $u_{i,j} = 0$), the phase angle between the two end buses of this line will be enforced to be 0, which is not logical for the power flow in the network. Constraint (35) limits the generator ramp between two successive periods. Constraint (36) gives the lower and upper boundaries of the amount of base load that can be shedded at each bus. Constraint (37) ensures that the flow generated by generators is within their capacity. Constraint (38) limits the number of lines that can be switched. Constraints (39) - (40) state $u_{i,j}$ and $LS^{dc}_{j,t}$ are binary decision variables.

2.3. Reconfiguring traffic-power system

In this subsection, we assume that the independent transportation network and PN are taken over by an emergency response department. Thus, it integrally operates and reconfigures the traffic-power networks to minimize the total system performance loss.

In this situation, the EV charging load $p^{dc}_j(t)$ at each bus becomes a decision variable, which can be calculated by the following equation:

$$p^{dc}_j(t) = \sum_{a \in M(j)} \sum_{s \in \mathcal{N}_S} \sum_{c \in \mathcal{C}} \sum_{e \in \mathcal{E}_c} p^{ev}_a [UE^{s,e}_{a,c}(t) - VE^{s,e}_{a,c}(t)] \tag{41}$$

where $M(j)$ is a mapping from bus set $\mathcal{P}_N$ to charging links set $\mathcal{A}_C$, which specifies the connection between buses in a power system and charging links in a RN.

Since the traffic-power system is integrally operated, the charging locations and times of EVs can be flexibly arranged to assist minimizing the

objective. Therefore, it is not necessary to have variable $LS_{j,t}^{dc}$ anymore to control whether the EV charging load is shedded or not. Eq. (30) is rewritten as follows:

$$p_{j,t}^{g} + \sum_{i \in \Gamma^{-}(j)} P_{i,j,t} - \sum_{k \in \Gamma^{+}(j)} P_{j,k,t} = p_{j,t}^{b} - LS_{j,t}^{b} + p_{j,t}^{dc}, \forall j \in \mathcal{P}_N \tag{42}$$

The whole problem is formulated as follows:

$$\min_{\boldsymbol{z} \in \Psi} P_I = \sum_{s \in \mathcal{N}_S} \sum_{t \in \mathcal{T}} \sum_{a \in \mathcal{A}_S} [DG_a^s(t) - UG_a^s(t) + \sum_{c \in \mathcal{C}} \sum_{e \in \mathcal{E}_c} (DE_{a,c}^{s,e}(t) - UE_{a,c}^{s,e}(t))] \cdot \phi + \sum_{t \in \mathcal{T}} c_j^b \cdot LS_{j,t}^b \tag{43}$$

where $\Psi = \{z|$ s.t. (11) - (27), (31) - (39) and (41) - (42)$\}$.

In each time period, there are expected demand $E(t)$ and unsatisfied demand $\Delta E(t)$ in the system. The following equation is employed to measure the system performance $P(t)$ [1]:

$$P(t) = \frac{E(t) - \Delta E(t)}{E(t)} \tag{44}$$

where $0 \geq \Delta E \geq E$. This equation can be understood as the percentage of demand that can be satisfied in the system in period t.

In the studied traffic-power system, the expected demand includes the all vehicle types traffic demand over all OD pairs and base electricity demand over all buses, which is formulated as follows:

$$E(t) = \sum_{s \in \mathcal{N}_S} \sum_{a \in \mathcal{A}_S} [DG_a^s(t) + \sum_{c \in \mathcal{C}} \sum_{e \in \mathcal{E}_c} DE_{a,c}^{s,e}(t)] \cdot \phi + \sum_{j \in \mathcal{P}_N} c_j^b \cdot p_{j,t}^b \tag{45}$$

where time value ϕ and shedding load cost c_j^b are used so that the system performance of PNs and RNs have the same physical dimension, thus, additivity. It can be understood as if these demands are satisfied, the corresponding amount of money can be saved.

The only difference between ΔE and Eq. (43) is without summation over

time. Eq. (46) is rewritten as follows:

$$P(t) = \frac{\sum_{s\in\mathcal{N}_S}\sum_{a\in\mathcal{A}_S}[UG_a^s(t) + \sum_{c\in\mathcal{C}}\sum_{e\in\mathcal{E}_c} UE_{a,c}^{s,e}(t)]\cdot\phi + \sum_{j\in\mathcal{P}_N}[p_{j,t}^b - LS_{j,t}^b]\cdot c_j^b}{\sum_{s\in\mathcal{N}_S}\sum_{a\in\mathcal{A}_S}[DG_a^s(t) + \sum_{c\in\mathcal{C}}\sum_{e\in\mathcal{E}_c} DE_{a,c}^{s,e}(t)]\cdot\phi + \sum_{j\in\mathcal{P}_N} c_j^b\cdot p_{j,t}^b} \tag{46}$$

3. Case study

The modified IEEE 14-bus system is used as the PN part in this study. It is preventive of small-size power systems and the original IEEE 14-bus test case is a portion of the American electric power system (in the Midwesten US) [40]. There are 14 buses and 20 transmission lines, and the detailed data can be found in Ref. [41]. The transportation network part is illustrated by a partial highway network in North Carolina (NC), U.S., which is shown in Figure 3. Figure 2(a) shows the locations of EV charging stations within this area and the geographic data of the highway network are collected from Google map. This partial highway network is abstracted into an approximated topology network as shown in Figure 2(b). The number along the link is the link ID. In spite of its relatively small scale, the system is complete enough to illustrate the proposed models. There are 9 fast-charging stations in the studied highway network and their connections to the served buses are listed in Table 1. The data used in this studied is detailed in Appendix A.

The proposed model is illustrated by solving and analyzing the following hypothetical scenario: it is reported that links 4, 17, 19 in the highway network and lines 2-3, 2-4, 7-8 in the PN are destroyed, and they cannot provide services normally. The problem that the emergency response department face is how to reconfigure and operate both the traffic and power systems, so that their performance loss caused by the disruption can be minimized during the peak hours (i.e., 17:00-18:59).

All of the experiments have been run on a computer with an Intel Core i7-8700 3.2-GHz CPU with 32 GB of RAM. All of the problems have been solved by the commercial software IBM ILOG CPLEX (version 20.1.0.0).

3.1. The impact of the different response resource level

In this subsection, 5 different resource levels are investigated: $N_h = N_u =$ 0, 1, 2, 3, 4, 5. Figure 3.1 shows the system performance level evolution over the studied time horizon under different resource levels. Time step = 0 denotes the occurrence of the reconfiguration. In this period, it can be found

Table 1: Connections between charging links and Buses

Charging link	Bus	$NC_a(t)$
301	2	30
302	3	45
303	4	30
304	5	30
305	6	30
306	7	15
307	8	30
308	9	15

that the system performance levels are different under different resource levels. It is because that once the transmission network topology is reconfigured, the effects (i.e., the shedded load) are influenced immediately. Whereas, the effects of reconfiguring highway networks are taken into account in the following time steps, since the delay is resulted from the time required from origins to destinations for vehicles. The performance level denotes the percentage of the total demand is satisfied. As expected, the system performance increase with the resource levels. If the response resource level increase from 0 to 2, the system performance can be largely increased from 76.58% to 86.26%. After that, the marginal economic benefit of additional response resource reduces as the number of links reversing and lines switching raises. This is also can be found in Figure 3.1. When the resource level is 2, the nominal cost of both highway networks and transmission networks reduces largely. It also shows the effectiveness of reconfiguring network topology during the restoration period. Table 3.1 shows the reconfiguration solutions of links in the RNs and that of lines in the PNs. From the third to the fifth columns, they represent the number of vehicles, GVs and EVs arrived at destinations in the end of the studied horizon. The last column represents the total charging demand during the studied horizon. The Third column in Table 3.1 shows that the optimal set of the switched lines in low resource level scenarios is not necessarily a subset of the switched lines in high resource level scenarios. For instance, line 4-7 is switched off when resource level is 1, whereas lines 4-9 and 7-9 are switched off when resource level increase to 2. However, this is not applied in RNs in this example. There could be two reasons resulted from the traffic demand distribution: 1) The used gravity model generates high traffic demand between two cities where their distance is short and pop-

Table 2: Solutions under different resource levels

Resource levels	$h_a = 1$	$u_{i,j} = 0$	Vehicles	GVs	EVs	Charging demand (MW)
0			19091	17336	1755	182.8
1	117	4-7	22142	20322	1820	148.8
2	104,117	4-9,7-9	21573	19512	2061	165.68
3	5,104,117	4-7,4-9,6-13	21987	19656	2331	207.68
4	5,26,114,117	4-7,4-9,1-2,9-14	22005	19669	2336	222.88
5	5,25,26,114,117	4-7,4-9,1-2,6-12,13-14	21999.5	19656	2343.5	201.28

ulation is large. This may cause high traffic volume on some certain two-way road sections; 2) To model the directional differences of traffic volumes, the direction of traffic demand between two cities is randomly selected. It could make the bidirectional high traffic volumes become one-way high traffic volumes on some road sections. Therefore, once these links with high traffic volumes are damaged (e.g., links 17 and 19), they may alway have priorities to be restored so that the system loss can be minimized. Moreover, when there are large volume differences between two opposite links, the link capacity can be greatly improved by reversing the link with less volumes (e.g., links 5 and 26). Less nominal cost of system performance loss and higher resource level do not mean more vehicles can arrive the destinations during the studied period. For example, Figure 3.1 shows the nominal loss cost of resource level being 2 is less than that of resource level being 1. However, Table 3.1 shows that there are also less arrivals when the resource level is 2 than when the resource level is 1. It is because the vehicles arrive their destinations earlier when the resource level is 2 than when the resource level is 1. There is a trade-off between the number of arrivals and their travel time for RNs.

3.2. Different EV penetration levels and decision environments

Without loss of generality, both the maximum number of lines can be switched and links can be reversed are set to be 3 (i.e., $N_u = 3$ and $N_h = 3$). When RNs and PNs independently optimize their restoration plans, we assume that the operators of RNs share their temporal and spatial charging demand with the PNs operators first at the beginning of the restoration horizon and they no longer change their plans. This situation can be regarded as the unmanaged charging demand scenarios from the PNs operator's perspective. In this case, the PNs operators have to satisfy all EV charging demand and only the base electricity load can be shedded when they optimize their

Table 3: Solutions under different EV penetration levels and decision environments

EV Penetration	Environments	$h_a = 1$	$u_{i,j} = 0$	Total cost ($)	Cost for RNs ($)	Cost for PNs ($)	Vehicles	GVs	EVs	Charging demand (MW)
0%	Interdependent	5,104,117	4-7,4-9,6-13	773300	729300	44000	30540	30540	0	0
	Independent	- *	4-9,7-9,13-14	773300	729300	44000	22142	30540	0	0
25%	Interdependent	5,104,117	4-7,4-9,6-13	821260.15	775340.15	45920	26933.5	25346	1587.5	166.4
	Independent	-	4-7,4-9,9-14	824392.15	770192.15	54200	21987	19656	2331	255.2
50%	Interdependent	5,104,117	4-7,4-9,6-13	894274.2	845226.2	49048	21987	19656	2331	207.68
	Independent	-	4-7,4-9,13-14	897389.5	843069.5	54320	21999.5	19656	2343.5	294
75%	Interdependent	11,109,117	4-7,4-9,6-13	994669.5	945509.5	49160	13980	11325	2655	218.4
	Independent	-	4-7,4-9,13-14	998,262	943462	54800	14430	10437	3105	318
100%	Interdependent	22,102,117	4-7,4-9	1133009	1083849	49160	2822.5	0	2822.5	210
	Independent	117	4-7,4-9,13-14	1134561.5	1081801.5	52760	3272.5	0	3272.5	243.6

* The solution is same to the interdependent environment

restoration plans.

Figure 3.2 shows the traffic-power systems performance evolution over restoration horizon under different EV penetration levels. Table 3 shows the benefit of line switching and link reversing in terms of system performance loss for different EV penetration levels and different decision-making environments. As shown in Figure 3.2, the traffic-power system performance decreases as the EV penetration increases. When EV penetration increase from 0% to 100%, the nominal total costs of the traffic-power system increases from $773300 to $1133009, leading to a 46.7% increase in costs. Extra charging time needed for EVs comparing to GVs and the limited chargers are the main reasons of this result. When the EV penetration is equal to or less than 50%, the reconfiguration solutions are stable for both the traffic-power systems and the independently optimized RNs. In this situation, links 5, 104 and 117 in RNs are reversed. Lines 4-7, 4-9 and 6-13 are always switched off, when the restoration plans of PNs are coordinately optimized. When there are no EV in RNs, no matter interdependently or independently plan the restoration of RNs and PNs, both of them have the same nominal total system performance costs. When EVs arise in RNs, the nominal total costs of interdependently planing the traffic-power system are lower than that of independently planing them. It shows the added values of coordinately optimize the two networks. The total charging demand over the studied horizon in the last column in Table 3 shows the difference between coordinately managing the EV charging demand and independently managing them from the perspective of the RNs' operator. The coordinately scheduled spatiotemporal charging demand is a trade-off between RNs and PNs in terms of their individual system performance loss.

4. Conclusion

In this paper, the mathematic models of independently reconfiguring road networks (RNs) and power networks (PNs) are proposed to minimize the system performance loss during the restoration period. In both networks, system performance loss was measured by the unsatisfied demand, i.e., cumulative unsatisfied gasoline vehicles (GVs) and electric vehicles (EVs) traffic demand for RNs and cumulative shedded electricity load for PNs over the studied period. For RNs, the proposed model was to solve the system optimal dynamic traffic assignment problem considering the characteristics of EVs and fast-charging stations (FCCSs). These characteristics include driving range (battery capacity) and state of charge (SoC) of EVs, and physical constraints in FCSs, such as number of chargers and charging power. Moreover, a two-stage mixed integer optimization model was proposed to minimize the integrated system performance loss duration the restoration period. In the tactical level, reconfiguration solutions for the traffic-power systems are solved to enhance the system resilience after a disruptive event. In the operational level, an integrated traffic-power systems model was proposed to describe the dynamic interdependency between the PNs and RNs networks. The two networks were coupled through the spatial and temporal EV charging demand, which is coordinately managed in the proposed model. A partial highway network in North Carolina (NC), USA and modified IEEE 14-bus system were used to illustrate the proposed methods. The results showed that: 1) applying reconfiguration strategies on PNs and RNs during restoration period could effectively improve the system performance after disruptions; 2) the system performance loss could be largely mitigated by coordinately reconfiguring the traffic-power systems and managing EV charging demand, comparing to independently plan the reconfiguration solutions for PNs and RNs; 3) with the increasing of EV penetrations, the efficiency of the RNs decreased significantly, which hinted that more FCSs needed to be deployed in this area. The proposed models could be employed to provide effective reconfiguration solutions (i.e., links reversing in RNs and lines switching in PNs) for traffic-power systems during restoration period to enhance the system resilience. Operational solutions (i.e., system optimal dynamic traffic assignment and optimal power flow distribution) could be served as a benchmark to mange thee traffic-power flow and EV charging demand.

This work can be extended in several directions: 1) Replacing system optimal by user equilibrium in dynamic traffic assignment problem is valuble

but challenging for the traffic-power systems model, although such model may not be suitable to apply into emergency response problem. It is because satisfying user equilibrium conditions mean more complicated optimization model and extremely expensive computational cost. 2) Including mobile energy storage systems (MESSs) into emergency response strategies could be an effective way to improve the resilience of RNs. However, how to integrate MESSs into the traffic-power system model still need more efforts; 3) EVs are assumed to only replenish batteries in FCSs, in this paper. Bidirectional transmission electricity service in FCSs can be considered to more efficiently operate the traffic-power systems and strengthen their resilience.

Appendix A. Data discription

A partial highway network in NC, USA is shown in Figure 3. The used parameters of this studied network are listed in Tables A.4 and A.5. The node ID, its corresponding town or city name and its population within this area are listed in Table A.6. The cities or towns attached source-sink nodes are those whose population is more than 11000. According to their geographic distances among these nodes and their population, the gravity model is used to generate the daily traffic demand. The generic form of gravity model [42] is usually written as $f_{od} = P_o^{\alpha} P_d^{\beta} / D_{od}^{\gamma}$, where P_o and P_d are the population sizes of origin a and destination d, D_{od} is the shortest distance between them, α, β and γ are fitting parameters. We set $\alpha = \beta = 0.92$ and $\gamma = 1$, in this study. To consider the worst-case scenario, the traffic volumes at 17:00 and 18:00 are adopted, which are the peak and account for approximately 15.3% of the daily traffic, in the basic time-of-day patterns [43]. The traffic volumes usually show the directional differences and it is difficult to get the applicable statistics for time-of-day travel by direction for each O-D pair [43]. For simplicity, only one direction is randomly selected for each O-D pair and traffic volumes in the other direction is ignored. The obtained traffic demand is shown in Table. A.7. According to Ref. [44], the electricity demand in U.S. has the similar peak hours with traffic volumes and their demand does not change a lot during this period. For simplicity, it is assumed that the base load at each bus is constant during this period and follows the standard test data [41].

Table A.4: Parameters of the studied highway network

Link ID	Start	End	ν_a	β_a	ρ_a	Type	$L_a k_{jam}$	If_a/Of_a	Lanes
1/101	2/1	1/2	5	10	5	G	13910	500	2
2/102	2/3	3/2	3	6	3	G	8346	500	2
3/103	3/8	8/3	4	8	4	G	5564	250	1
4/104	1/5	5/1	3	6	3	G	8346	500	2
5/105	2/5	5/2	3	6	3	G	8346	500	2
6/106	2/6	6/2	3	6	3	G	8346	500	2
7/107	3/4	4/3	1	2	1	G	1391	250	1
8/108	5/6	6/5	1	2	1	G	2782	500	2
9/109	4/6	6/4	3	6	3	G	4173	250	1
10/110	4/7	7/4	2	4	2	G	2782	250	1
11/111	4/8	8/4	3	6	3	G	4173	250	1
12/112	6/7	7/6	5	10	5	G	13910	500	2
13/113	6/7	7/6	5	10	5	G	6955	250	1
14/114	7/8	8/7	2	4	2	G	5564	500	2
15/115	7/8	8/7	2	4	2	G	2782	250	1
16/116	1/10	10/1	4	8	4	G	11128	500	2
17/117	10/14	14/10	3	6	3	G	8346	500	2
18/118	5/15	14/5	5	10	5	G	6955	250	1
19/119	11/14	14/11	2	4	2	G	5564	500	2
20/120	5/9	9/5	2	4	2	G	5564	500	2
21/121	6/9	9/6	2	4	2	G	5564	500	2
22/122	9/11	11/9	2	4	2	G	5564	500	2
23/123	11/9	9/11	2	4	2	G	5564	500	2
24/124	11/12	12/11	4	4	4	G	11128	500	2
25/125	6/12	12/6	4	4	4	G	11128	500	2
26/126	12/13	13/12	3	6	3	G	4173	250	1
27/127	7/13	13/7	2	4	2	G	2782	250	1
29/129	2/201	201/2	0	0	0	S/R	inf	inf	
30/130	10/202	202/10	0	0	0	S/R	inf	inf	
36/136	5/203	203/5	0	0	0	S/R	inf	inf	
31/131	11/204	204/11	0	0	0	S/R	inf	inf	
32/132	12/205	205/12	0	0	0	S/R	inf	inf	
33/133	14/206	206/14	0	0	0	S/R	inf	inf	
34/134	8/207	207/8	0	0	0	S/R	inf	inf	
35/135	3/208	208/3	0	0	0	S/R	inf	inf	

Table A.5: Parameters of the studied traffic-power system

Parameters	Values
v_f (m/h)	65
k_{jam}(veh/m)	214
δ (min)	6
q_{max} (veh/h/lane)	2500
p_a^{ev} (kW)	80
η (kMh/mile)	0.4
ϕ ($/h)	13
C	1
E_c	10
α_a^t (ELs/δ)	3
Initial EL of EV	3

Table A.6: Population of the towns and cities

Node ID	Name	Population	Node ID	Name	Population
1	Zebulon	4526	2	Rocky Mount	56650
3	Tarboro	11255	4	Pinetops	1351
5 & 6	Wilson	49436	7	Farmville	4695
8	Greenville	86142	9	Kenly	1344
10	Raleigh	418099	11	Selma & Smithfield	17901
12	Goldsboro	35609	13	Snow Hill	1611
14	Clayton	16529			

References

[1] Y.-P. Fang, G. Sansavini, Optimum post-disruption restoration under uncertainty for enhancing critical infrastructure resilience, Reliability Engineering & System Safety 185 (2019) 1–11.

[2] S. Ma, B. Chen, Z. Wang, Resilience enhancement strategy for distribution systems under extreme weather events, IEEE Transactions on Smart Grid 9 (2) (2016) 1442–1451.

[3] C. R. Center, Post event report: Henan flood – july 17-21, https://www.gccapitalideas.com/2021/07/28/post-event-report-henan-flood-july-17-21/, accessed August. 20, 2021 (2021).

Table A.7: O-D pairs and their traffic demand

Link ID	Node ID	Demand	Link ID	Node ID	Demand
130	203	6460	136	204	620
129	202	5700	129	208	620
130	206	5500	133	203	460
134	202	5380	131	205	460
130	205	3720	133	204	460
131	202	3560	131	201	400
136	201	2400	134	204	380
129	207	1720	129	206	320
136	207	1520	136	208	320
134	205	1120	133	205	280
130	208	960	134	206	260
132	203	940	132	208	160
132	201	760	135	204	100
135	207	680	135	206	60

[4] A. A. Ganin, M. Kitsak, D. Marchese, J. M. Keisler, T. Seager, I. Linkov, Resilience and efficiency in transportation networks, Science advances 3 (12) (2017) e1701079.

[5] X. Zhang, S. Mahadevan, S. Sankararaman, K. Goebel, Resilience-based network design under uncertainty, Reliability Engineering & System Safety 169 (2018) 364–379.

[6] C. Zhu, J. Wu, M. Liu, J. Luan, T. Li, K. Hu, Cyber-physical resilience modelling and assessment of urban roadway system interrupted by rainfall, Reliability Engineering & System Safety 204 (2020) 107095.

[7] H. Wang, A. F. Abdin, Y.-P. Fang, E. Zio, Resilience assessment of electrified road networks subject to charging station failures, Computer-Aided Civil and Infrastructure Engineering`doi:https://doi.org/10.1111/mice.12736`.

[8] T. Aziz, Z. Lin, M. Waseem, S. Liu, Review on optimization methodologies in transmission network reconfiguration of power systems for grid resilience, International Transactions on Electrical Energy Systems 31 (3) (2021) e12704.

[9] Y. Wang, A. O. Rousis, G. Strbac, On microgrids and resilience: A comprehensive review on modeling and operational strategies, Renewable and Sustainable Energy Reviews 134 (2020) 110313.

[10] D. Fan, Y. Ren, Q. Feng, Y. Liu, Z. Wang, J. Lin, Restoration of smart grids: Current status, challenges, and opportunities, Renewable and Sustainable Energy Reviews 143 (2021) 110909.

[11] H. Sekhavatmanesh, R. Cherkaoui, Distribution network restoration in a multiagent framework using a convex opf model, IEEE Transactions on Smart Grid 10 (3) (2018) 2618–2628.

[12] H. Sabouhi, A. Doroudi, M. Fotuhi-Firuzabad, M. Bashiri, Electricity distribution grids resilience enhancement by network reconfiguration, International Transactions on Electrical Energy Systems (2021) e13047.

[13] P. Agrawal, N. Kanwar, N. Gupta, K. Niazi, A. Swarnkar, Resiliency in active distribution systems via network reconfiguration, Sustainable Energy, Grids and Networks 26 (2021) 100434.

[14] I. G. Guimaraes, D. P. Bernardon, V. J. Garcia, M. Schmitz, L. L. Pfitscher, A decomposition heuristic algorithm for dynamic reconfiguration after contingency situations in distribution systems considering island operations, Electric Power Systems Research 192 (2021) 106969.

[15] W. Li, Y. Li, C. Chen, Y. Tan, Y. Cao, M. Zhang, Y. Peng, S. Chen, A full decentralized multi-agent service restoration for distribution network with dgs, IEEE Transactions on Smart Grid 11 (2) (2019) 1100–1111.

[16] F. Liberati, A. Di Giorgio, A. Giuseppi, A. Pietrabissa, F. D. Priscoli, Efficient and risk-aware control of electricity distribution grids, IEEE Systems Journal 14 (3) (2020) 3586–3597.

[17] H. Sekhavatmanesh, R. Cherkaoui, Analytical approach for active distribution network restoration including optimal voltage regulation, IEEE Transactions on Power Systems 34 (3) (2018) 1716–1728.

[18] Y. Zhang, M. Bansal, A. R. Escobedo, Risk-neutral and risk-averse transmission switching for load shed recovery with uncertain renewable generation and demand, IET Generation, Transmission & Distribution 14 (21) (2020) 4936–4945.

[19] M. Nazemi, P. Dehghanian, Seismic-resilient bulk power grids: Hazard characterization, modeling, and mitigation, IEEE Transactions on Engineering Management 67 (3) (2019) 614–630.

[20] Y. Wang, J. Wang, Integrated reconfiguration of both supply and demand for evacuation planning, Transportation research part E: logistics and transportation review 130 (2019) 82–94.

[21] Y. Wang, J. Wang, Measuring and maximizing resilience of transportation systems for emergency evacuation, IEEE Transactions on Engineering Management 67 (3) (2019) 603–613.

[22] S.-W. Chiou, A traffic-responsive signal control to enhance road network resilience with hazmat transportation in multiple periods, Reliability Engineering & System Safety 175 (2018) 105–118.

[23] X. Koutsoukos, G. Karsai, A. Laszka, H. Neema, B. Potteiger, P. Volgyesi, Y. Vorobeychik, J. Sztipanovits, Sure: A modeling and simulation integration platform for evaluation of secure and resilient cyber–physical systems, Proceedings of the IEEE 106 (1) (2017) 93–112.

[24] Y. Wu, G. Hou, S. Chen, Post-earthquake resilience assessment and long-term restoration prioritization of transportation network, Reliability Engineering & System Safety 211 (2021) 107612.

[25] T. Zhao, Y. Zhang, Transportation infrastructure restoration optimization considering mobility and accessibility in resilience measures, Transportation Research Part C: Emerging Technologies 117 (2020) 102700.

[26] W. Wei, L. Wu, J. Wang, S. Mei, Network equilibrium of coupled transportation and power distribution systems, IEEE Transactions on Smart Grid 9 (6) (2017) 6764–6779.

[27] H. Wang, Y.-P. Fang, E. Zio, Risk assessment of an electrical power system considering the influence of traffic congestion on a hypothetical scenario of electrified transportation system in new york state, IEEE Transactions on Intelligent Transportation Systems 22 (1) (2021) 142–155.

[28] M. Nazemi, P. Dehghanian, X. Lu, C. Chen, Uncertainty-aware deployment of mobile energy storage systems for distribution grid resilience, IEEE Transactions on Smart Grid.

[29] S. Lei, C. Chen, Y. Li, Y. Hou, Resilient disaster recovery logistics of distribution systems: Co-optimize service restoration with repair crew and mobile power source dispatch, IEEE Transactions on Smart Grid 10 (6) (2019) 6187–6202.

[30] B. Taheri, A. Safdarian, M. Moeini-Aghtaie, M. Lehtonen, Distribution system resilience enhancement via mobile emergency generators, IEEE Transactions on Power Delivery.

[31] D. Anokhin, P. Dehghanian, M. A. Lejeune, J. Su, Mobility-as-a-service for resilience delivery in power distribution systems, Production and Operations Management.

[32] Y. Wang, Y. Xu, J. Li, C. Li, J. He, J. Liu, Q. Zhang, Dynamic load restoration considering the interdependencies between power distribution systems and urban transportation systems, CSEE Journal of Power and Energy Systems 6 (4) (2020) 772–781.

[33] S. Yao, P. Wang, X. Liu, H. Zhang, T. Zhao, Rolling optimization of mobile energy storage fleets for resilient service restoration, IEEE Transactions on Smart Grid 11 (2) (2019) 1030–1043.

[34] B. Li, Y. Chen, W. Wei, S. Huang, S. Mei, Resilient restoration of distribution systems in coordination with electric bus scheduling, IEEE Transactions on Smart Grid.

[35] International Energy Agency (IEA), Global ev outlook 2020, Tech. rep., IEA (June 2020).

[36] S. A. Adderly, D. Manukian, T. D. Sullivan, M. Son, Electric vehicles and natural disaster policy implications, Energy Policy 112 (2018) 437–448.

[37] K. Feng, N. Lin, S. Xian, M. V. Chester, Can we evacuate from hurricanes with electric vehicles?, Transportation research part D: transport and environment 86 (2020) 102458.

[38] I. Yperman, The link transmission model for dynamic network loading.

[39] X. Zhang, S. Mahadevan, K. Goebel, Network reconfiguration for increasing transportation system resilience under extreme events, Risk analysis 39 (9) (2019) 2054–2075.

[40] U. Washington, Power systems test case archive, http://labs.ece.uw.edu/pstca/pf14/pg_tca14bus.htm, accessed August. 13, 2021 (2021).

[41] Y. Fang, G. Sansavini, Optimizing power system investments and resilience against attacks, Reliability Engineering & System Safety 159 (2017) 161–173.

[42] Y. Ren, M. Ercsey-Ravasz, P. Wang, M. C. González, Z. Toroczkai, Predicting commuter flows in spatial networks using a radiation model based on temporal ranges, Nature communications 5 (1) (2014) 1–9.

[43] M. Hallenbeck, M. Rice, B. Smith, C. Cornell-Martinez, J. Wilkinson, Vehicle volume distributions by classification, Tech. rep. (1997).

[44] U. E. I. Administration, Hourly electric grid monitor, https://www.eia.gov/electricity/gridmonitor/dashboard/electric_overview/US48/US48, accessed August. 14, 2021 (2021).

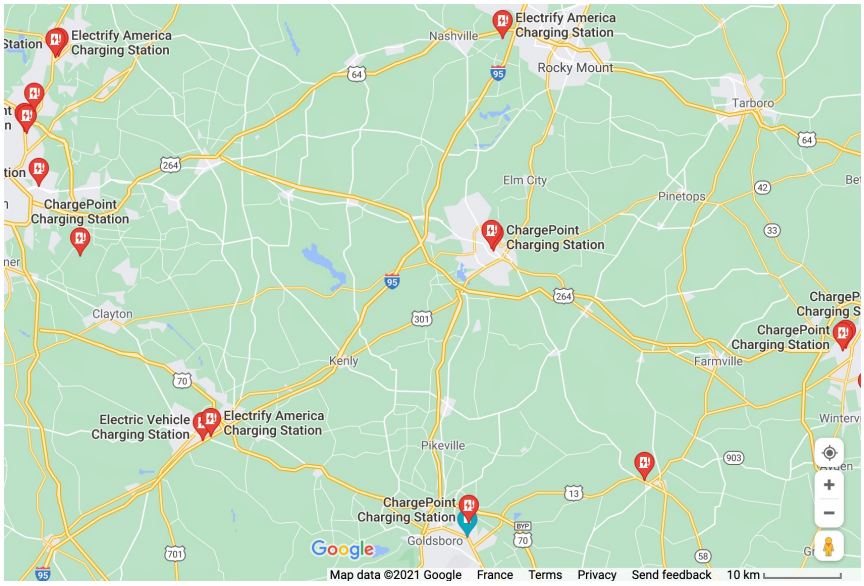

(a) The partial highway network in NC

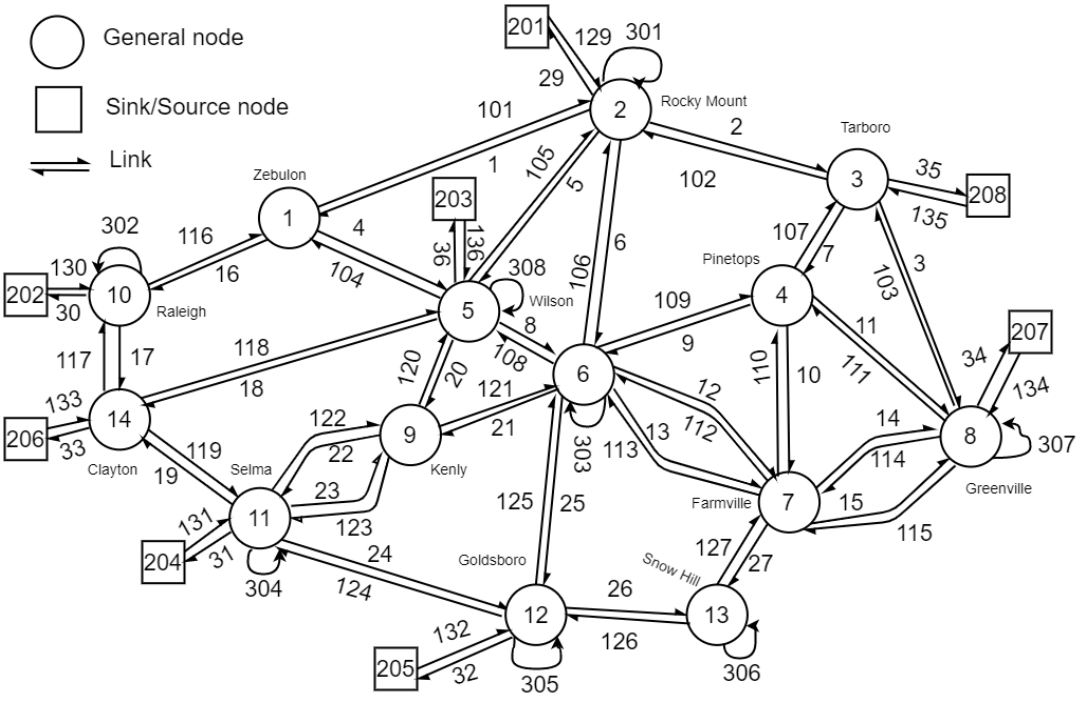

(b) The approximated topology network

Figure 2: The studied highway network

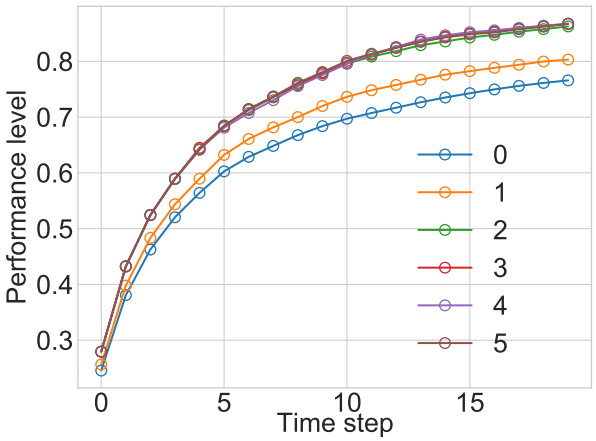

Figure 3: System performance evolution over restoration horizon under different resource level

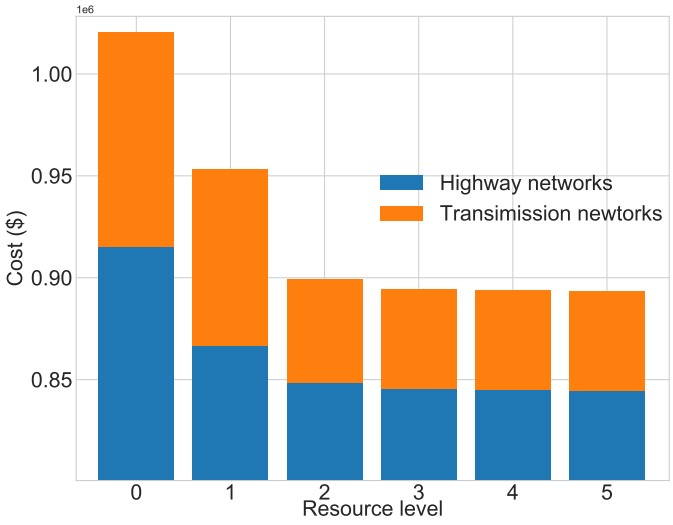

Figure 4: Nominal cost for the studied traffic-power systems under different resource level

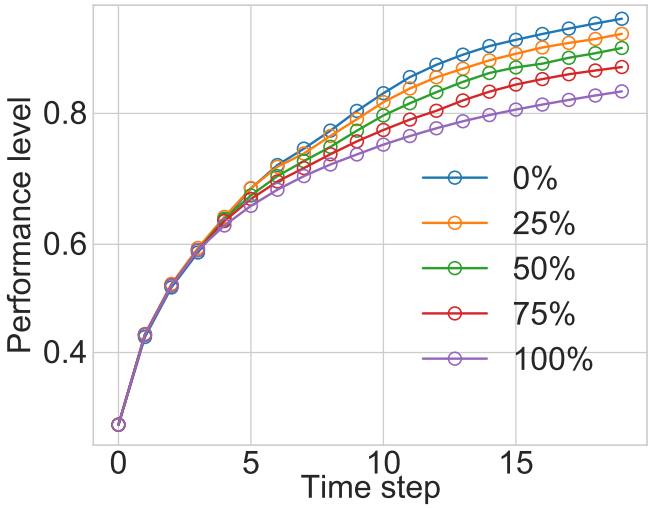

Figure 5: The traffic-power systems performance evolution over restoration horizon under different EV penetration levels